

Validated Performance Prediction of Adsorption Chillers: Bridging the Gap from Gram-Scale Experiments to Full-Scale Chillers

Stefan Graf, Sebastian Eibel, Franz Lanzerath, and André Bardow*


Adsorption chillers provide sustainable cooling from waste or solar heat. However, adsorption chillers currently show limited performance. To increase the performance, new working pairs and adsorber geometries are constantly proposed. Evaluating the performance of new working pairs and adsorber geometries requires time and large amounts of the material. To reduce time and material needs, a method is presented to reliably predict the heat flows in the adsorber, specific cooling power (SCP), and coefficient of performance (COP) in an adsorption chiller from only 1 g of adsorbent material. For this purpose, the small-scale Infrared-Large-Temperature-Jump experiment is combined with a full-scale adsorption chiller model. The adsorption chiller model allows determining time-resolved heat flows, SCP, and COP. The prediction results are compared with a full-scale experiment of an adsorption chiller. For various process conditions, the prediction is highly reliable with average deviations of 18.5% for the heat flows, 1.4% for the SCP, and 7.0% for the COP compared with the experiment. The presented method allows a comprehensive and reliable evaluation of new working pairs and adsorber designs from only small amounts of the adsorbent material, thus guiding material improvements at an early stage of development.

1. Introduction

Sustainable cooling can be provided by adsorption chillers driven by thermal energy.^[1] Thermal energy can be provided either from waste heat or solar heat, reducing fossil consumption.^[2]

Dr. S. Graf, S. Eibel, Dr. F. Lanzerath, Prof. A. Bardow
Institute of Technical Thermodynamics
RWTH Aachen University
Schinkelstraße 8, 52062 Aachen, Germany
E-mail: andre.bardow@itt.rwth-aachen.de

Prof. A. Bardow
Institute of Energy and Climate Research – Energy Systems Engineering (IEK-10)
Forschungszentrum Jülich GmbH
Wilhelm-Johnen-Straße, 52425 Jülich, Germany

 The ORCID identification number(s) for the author(s) of this article can be found under <https://doi.org/10.1002/ente.201901130>.

© 2020 The Authors. Published by WILEY-VCH Verlag GmbH & Co. KGaA, Weinheim. This is an open access article under the terms of the Creative Commons Attribution-NonCommercial License, which permits use, distribution and reproduction in any medium, provided the original work is properly cited and is not used for commercial purposes.

DOI: 10.1002/ente.201901130

However, today, adsorption chillers still suffer from low specific cooling powers (SCPs) and low coefficient of performances (COPs).^[3] To improve the SCP and COP of adsorption chillers, new working pairs and adsorber geometries are continuously proposed.^[4]

Determining the SCP and COP for new working pairs and adsorber geometries usually requires a full-scale adsorption chiller setup, consisting of adsorber, condenser, and evaporator.^[5] However, constructing and operating full-scale setups is time-consuming and expensive: testing new geometries requires usually labor-intensive manual manufacturing of the full-scale adsorbers. The infrastructure needed to run a full-scale adsorber is high for heat supply and removal. Furthermore, novel adsorbent materials are available often only in small amounts that are insufficient for evaluation in a full-scale adsorption chiller on the kilogram scale. For example, currently, intensively discussed metal-organic frameworks (MOFs) are

often more complex to synthesize than, e.g., zeolites and therefore are often also much more expensive.^[6]

To reduce time and material needs, dynamic modeling and simulation of adsorption chillers is often used. By modeling a full-scale adsorption chiller with all its components, simulations directly yield the SCP and COP.^[7–9] Because dynamic models of adsorption chiller are rather easy to set up,^[10] they are widely used to study the influence of process inputs,^[11] component designs,^[12,13] cycle designs,^[14] or control^[15] on SCP and COP. Models for full-scale adsorption chillers are often implemented as lumped-parameter models.^[9,16–18] Lumped-parameter models are simpler to implement than distributed 2D or 3D models^[19] and need less computational time.

However, dynamic models need to be calibrated and validated with experimental data to reliably predict the SCP and COP.^[20] So far, adsorption chiller models are calibrated and validated with experiments using full-scale adsorption chillers. Schicktzan and Núñez^[16] developed a dynamic model of an adsorption chiller and parametrized the model with information of the real adsorber geometry. However, two parameters needed to be calibrated with experimental data: 1) the effective heat transfer coefficient between the adsorbent and the adsorber heat exchanger, and 2) the effective diffusion coefficient from the

vapor vessel into the adsorbent. Heat transfer and diffusion coefficients depend strongly on the specific configuration of the adsorber.^[21–23] Thus, the coefficients need to be determined in the actual adsorber geometry. For this purpose, the heat transfer and diffusion coefficients are usually fitted so that the squared deviations are minimal between simulated and experimental pressures and temperatures in the adsorber. Schickanz and Núñez^[16] achieved deviations between the simulated and measured SCP of 5% and between the simulated and measured COP of 6%. Both values lie within the measurement uncertainty of the experiment.

Lanzerath et al.^[9] chose a similar calibration approach achieving a very high accuracy of simulated and measured SCP (difference 3%) and COP (difference 7.2%). In addition, the authors predicted the SCP and COP for other conditions (temperatures of adsorber, evaporator, and condenser and cycle times) than the conditions used for fitting heat transfer and diffusion coefficients. Average deviations for the predicted SCP were at 4.3% and for the predicted COP at 7.2%, both within the standard deviation of measurements. Thus, dynamic models calibrated to full-scale setups have been shown to extrapolate with excellent accuracy to other operating conditions.

Several other studies modeled full-scale adsorption chiller setups and compared the results with experiments.^[17,18,24–29] The diffusion coefficient is often taken from the literature. Unfortunately, the studies do not mention the method used to determine the heat transfer coefficient. Because the origin of the heat transfer coefficient is unclear, we believe that the heat transfer coefficient is also fitted to the experimental data as in the studies mentioned previously. Wang et al.^[17] also determined the deviation of the SCP and COP between experiment and simulation to 7.5% and 12%, respectively.

In short, calibrated models allow accurate predictions of the SCP and the COP for other operating conditions than those used for calibration and can thus reduce measurement time. However, calibration still requires a complete adsorption chiller experimental setup with usually several kilos of adsorbent material. Then, the benefits of dynamic modeling diminish. In addition, the models are only valid for one specific adsorber geometry because only effective heat transfer and diffusion coefficients are determined.^[21]

In previous work, we, therefore, calibrated heat transfer and diffusion coefficients in a full-scale adsorption chiller model with data from a simpler experimental setup: the Gravimetric Large-Temperature-Jump (G-LTJ) experiment.^[30] With the G-LTJ experiment, we studied a representative adsorber part.^[31] We used the data for temperature and loading from the G-LTJ experiment to fit heat transfer and diffusion coefficients in an adsorber model. Then, the heat transfer and diffusion coefficients were used in a full-scale adsorption chiller model to predict the SCP and COP. Experimental effort is much smaller compared with full-scale adsorption chiller experiments. Still, a representative adsorber part is needed to capture the heat exchanger geometry.

In summary, current full-scale adsorption chiller models are valid for one specific adsorber geometry. Full-scale adsorption experiments are necessary to determine heat transfer and diffusion coefficients.

In this study, we present a model-based method that predicts power density SCP and COP of full-scale adsorption chillers

without requiring a full-scale adsorption chiller experiment. We extend the small-scale Infrared Large-Temperature-Jump (IR-LTJ) method to determine geometry-independent heat transfer and diffusion coefficients.^[32] The IR-LTJ method requires only a small amount of adsorbent material of 1 g. Here, we extend the IR-LTJ procedure to extract both the heat transfer coefficient within the bed and to the wall. This extension is achieved by several IR-LTJ experiments of different bed heights and a spatially resolved dynamic model. The heat transfer and diffusion coefficients are used to parametrize a full-scale adsorption chiller model. For this purpose, a 3D spatially discretized model is developed to capture the actual adsorber geometry. The adsorption chiller model allows to vary the cycle design and the geometry of the adsorber heat exchanger. We show that the adsorption chiller model predicts the performance of a full-scale adsorption chiller setup with high accuracy for heat flows, power density SCP, and COP.

The article is organized as follows: In Section 2, we describe the methods to determine geometry-independent heat transfer and diffusion coefficients and present the distributed-parameter models for the adsorption chiller. The model is used in a case study to predict heat flows, power density SCP, and COP of an adsorption chiller, and compared with experimental data of the full-scale adsorption chiller setup (Section 3). In Section 4, we summarize the results and conclude the article.

2. From Gram-Scale Experiments to Full-Scale Chillers

In this section, we first present our method to determine the effective heat transfer and diffusion coefficients. For this purpose, we conduct small-scale IR-LTJ experiments (step 1, Section 2.1; **Figure 1**). We use the data of the IR-LTJ experiments to calibrate a dynamic model of the experiment, yielding the heat transfer and diffusion coefficients. Second, we present the model for the full-scale adsorption chiller to determine heat flows, power density SCP, and COP (step 2, Section 2.2).

2.1. Determining Heat Transfer and Diffusion Coefficients

Our goal is to obtain heat transfer and diffusion coefficients that allow us to model different adsorber geometries. For this purpose, we decompose the heat transfer into the heat transfer coefficient between the heat exchanger and the adsorbent bed $U_{\text{sor-hx,eff}}$ and the effective heat conductivity in the adsorbent bed $k_{\text{sor,eff}}$ (**Figure 2**). To differentiate between the heat transfer coefficient $U_{\text{sor-hx,eff}}$ to the wall and the heat conductivity $k_{\text{sor,eff}}$ in the bed, we conduct two IR-LTJ experiments with different bed heights of the adsorbent. Mass transfer is modeled by an effective overall diffusion coefficient D_{eff} .

Because our goal in the current work is to model an adsorption chiller with a packed bed, we also place the adsorbent in a packed-bed configuration on a sample carrier in the IR-LTJ experiment. The packed bed has a defined bed height h_{bed} . We impose a temperature jump (decrease for adsorption and increase for desorption) on the adsorbent. For the adsorption experiment, the start and end temperatures correspond to the start and end temperatures of the adsorption phase in an ideal adsorption chiller cycle;

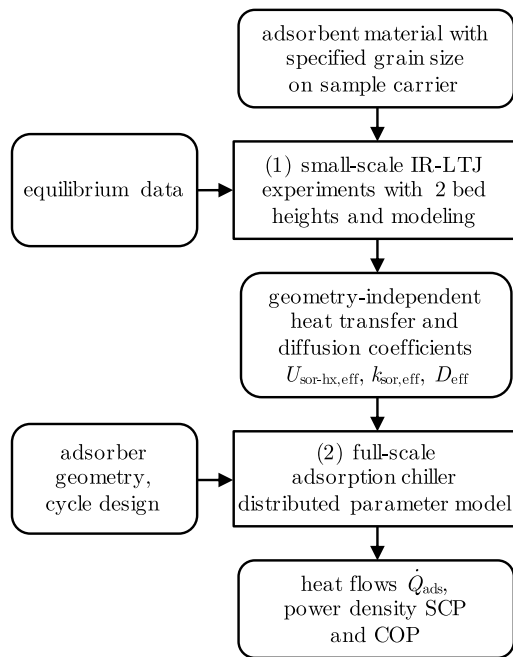


Figure 1. Combination of IR-LTJ experiment (step 1) with dynamic modeling of the adsorbent bed, resulting in geometry-independent effective heat transfer and diffusion coefficients. These coefficients are used in the distributed parameter model of the full-scale adsorption chiller (step 2) to determine heat flows in the adsorber \dot{Q}_{ads} , power density SCP and COP for a given adsorber geometry.

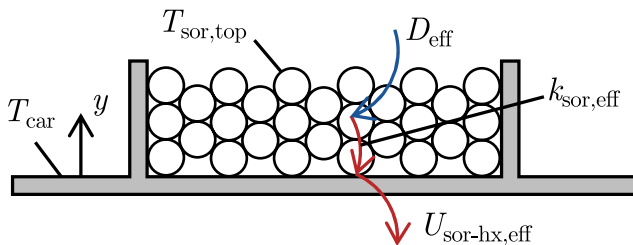


Figure 2. Adsorbent configuration (sor) on sample carrier (car) in IR-LTJ experiment. From IR-LTJ experiment and dynamic model, we determine the heat transfer and diffusion coefficients of the adsorbent bed: effective heat transfer between heat exchanger and adsorbent $U_{sor-hx,eff}$, effective heat conductivity through adsorbent bed $k_{sor,eff}$, and effective diffusion through adsorbent bed D_{eff} .

and for the desorption experiment to the desorption phase, respectively.^[33]

The temperature jump induces adsorption of water vapor from the constant vapor volume V . In the constant vapor volume, the pressure p_v thus decreases. The top surface temperature of the adsorbent $T_{sor,top}$ and the temperature of the sample carrier T_{car} are recorded with an infrared camera. In addition, the temperature of the vapor is measured with a PT 100 resistance thermometer T_v . The measurement uncertainty of the pressure sensor is $u_p = 5.78$ Pa, of the PT 100 resistance thermometer $u_{PT} = 0.031$ K and of the infrared camera $u_{IR} = 0.11$ K. Further information on the experimental setup, the measuring procedures, and measurement uncertainties can be found in Graf et al.^[32] In this former

study, we conducted a single experiment only without changing the height of the adsorber set. Therefore, we could only extract one effective heat transfer coefficient. However, the prediction of heat transfer in different adsorber geometries requires us to distinguish between the effective heat transfer coefficient to the heat exchanger and the thermal conductivity within the bed as presented by the extended IR-LTJ experiment in this study.

For the two different bed heights, the top surface temperature of the adsorbent $T_{sor,top}$ differs. For the experiment with the higher bed height, the temperature changes slower than for the experiment with the lower bed height due to the slower heat transfer through the higher packed bed. The differing temperature information for the two experiments allows distinguishing the two heat transfer coefficients $U_{sor-hx,eff}$ and $k_{sor,eff}$.

We use the pressure p_v and temperature T_v of the vapor, the top surface temperature of the adsorbent $T_{sor,top}$ and the sample carrier temperature T_{car} from the IR-LTJ experiments to determine the heat transfer and diffusion coefficients in a dynamic model of the experiment. The model of the IR-LTJ experiment consists of models for the adsorbent, heat transfer, mass transfer, and the vapor volume (Figure 3).

We discretize the dynamic model of the IR-LTJ experiment in vertical direction of the adsorbent bed y (cf., Figure 2) to distinguish between the effective heat transfer coefficient $U_{sor-hx,eff}$ to the heat exchanger and the thermal conductivity $k_{sor,eff}$ within the bed. We describe 1D heat transfer in the adsorbent bed by a partial differential equation for the energy balance^[34]

$$\underbrace{\rho_{sor}(c_{sor} + c_{ad}w)}_1 \frac{\partial T_{sor}}{\partial t} + \underbrace{\rho_{sor}u_{ad}}_2 \frac{\partial w}{\partial t} = \underbrace{k_{sor,eff}}_3 \frac{\partial^2 T_{sor}}{\partial y^2} + \underbrace{\rho_{sor}h_v}_{4} \frac{\partial w}{\partial t} \quad (1)$$

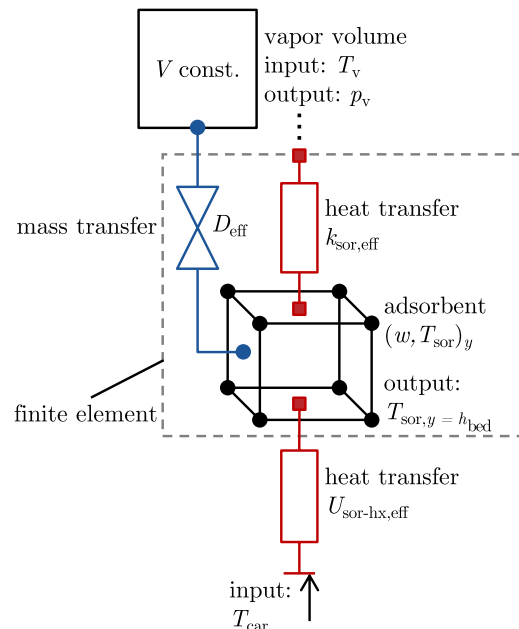


Figure 3. Dynamic model of extended IR-LTJ experiment. Model consists of models for adsorbent and vapor volume connected by heat and mass transfer models. The adsorbent bed is discretized into finite volumes in vertical (y) direction of the bed.

with 1) the change in internal energy from change in temperature $\frac{\partial T_{\text{sor}}}{\partial t}$, the density of the dry adsorbent ρ_{sor} , the specific heat capacity of the dry adsorbent c_{sor} and the adsorbed phase c_{ad} , and the loading w ; 2) the change in internal energy from change in loading $\frac{\partial w}{\partial t}$, the specific internal energy of the adsorbed phase u_{ad} ; 3) 1D heat flow by thermal conduction in the adsorbent bed with the thermal conductivity $k_{\text{sor,eff}}$ within the adsorbent bed; 4) the enthalpy flow rate of the adsorbate $\rho_{\text{sor}} h_v \frac{\partial w}{\partial t}$. To describe the adsorption equilibrium, that is, the equilibrium loading of the adsorbent $w(T, p)$ and the internal energy of the adsorbed phase $u_{\text{ad}}(w, T)$, we use the Dubinin model.^[32,35]

The boundary condition comes from thermal connection of the adsorbent bed with the sample carrier at $y=0$

$$k_{\text{sor,eff}} \frac{\partial T_{\text{sor}}}{\partial y} \Big|_{y=0} = U_{\text{sor-hx,eff}} (T_{\text{car}} - T_{\text{sor}}) \Big|_{y=0} \quad (2)$$

with the heat transfer coefficient $U_{\text{sor-hx,eff}}$ and the temperature of the sample carrier T_{car} .

In the mass balance of the adsorber, any convective mass flows are neglected and we assume only diffusive processes within each particle. In addition, we use the Linear-Driving-Force approach to describe the diffusion process.^[36] Then, the mass balance does not depend on the discretization in vertical direction y

$$\rho_{\text{sor}} \frac{\partial w}{\partial t} = \rho_{\text{sor}} \frac{15 D_{\text{eff}}}{r_{\text{particle}}^2} (w_{\text{eq}} - w) \quad (3)$$

with the effective diffusion coefficient D_{eff} , the adsorbent particle radius r_{particle} , and the equilibrium loading $w_{\text{eq}}(T_{\text{sor}}, p_v)$.

Modeling and simulation is conducted in the object-oriented and equation-based modeling language Modelica.^[37] Modelica does not allow directly implementing partial differential equations. Thus, we discretize the energy balance into finite volume elements in vertical direction y . The resulting discretized equations can be found in the Supporting Information.

The finite volume elements of the adsorber are connected to the vapor volume model. The vapor model describes the vapor phase with its constant volume V . In the constant volume, the vapor mass flow rate \dot{m}_{ad} to/from the adsorbent is related to the change in density of the vapor phase $\frac{d\rho}{dt}$

$$V \frac{d\rho(p_v, T_v)}{dt} = -\dot{m}_{\text{ad}} \quad (4)$$

The change in density of the vapor phase $d\rho/dt$ is a function of the measured vapor pressure p_v and the vapor temperature T_v . During adsorption, pressure decreases, reducing density. In this case, the mass flow rate \dot{m}_{ad} to the adsorbent is positive. During desorption, pressure increases, leading to a positive change in density and a negative mass flow rate \dot{m}_{ad} .

From the mass flow rate \dot{m}_{ad} , the change in loading $\frac{dw}{dt}$ and the actual loading w can be determined from a water mass balance around the adsorbent

$$\frac{dw}{dt} = \frac{1}{m_{\text{sor}}} \dot{m}_{\text{ad}} \quad \text{and} \quad (5)$$

$$w(t) = \int_0^t \frac{dw}{d\tau} d\tau + w_{\text{eq}}^{\text{initial}} \quad (6)$$

The initial loading of the adsorbent at the beginning of an experiment $w_{\text{eq}}^{\text{initial}}$ is determined from the equilibrium data at steady state pressure p_v^{initial} and temperature $T_{\text{sor}}^{\text{initial}}$.

The models are based on our library for adsorption-based energy systems SorpLib.^[10] For modeling of the fluid properties of water, we use the TILMedia library provided by TLK-Thermo GmbH.^[38] TILMedia uses the database REFPROP^[39] with data from Cox et al.^[40] and Chase^[41] to determine the fluid properties of water.

The models of the adsorbent are discretized in vertical direction y with a total number of discrete elements Y (cf., Figure 2). In this study, we choose ten discretization elements per millimeter $Y/h_{\text{bed}} = 10 \text{ mm}^{-1}$, which we identified as compromise between modeling accuracy and computational time (cf., Supporting Information).

In the case study, we investigate packed-bed configurations with a grain size diameter of $d_{\text{grain}} = 0.9 \text{ mm}$ and a bed porosity of $\epsilon_{\text{bed}} = 0.32$.^[13] We estimated the pressure drop over the adsorbent configuration for the case study by Darcy's law^[27,42] and found the pressure drop to be negligible. The cross-sectional area of the sample carrier is $A_{\text{bed,cross}} = 6.44 \times 10^{-4} \text{ m}^2$ and we assume the mean distance for the pressure drop δy be half of the bed height. For the case with the highest pressure drop, the mean distance becomes $\delta y = 1 \text{ mm}$, the vapor density $\rho_v = 0.94 \times 10^{-3} \text{ kg m}^{-3}$, the dynamic viscosity $\eta = 9.24 \times 10^{-6} \text{ Pa s}$, and the mass flow $\dot{m}_{\text{ad}} = 6.51 \times 10^{-7} \text{ kg s}^{-1}$, resulting in a maximum pressure drop of 2.6 Pa. Thus, compared with the absolute pressure of 1227 Pa, the pressure drop can be neglected.

If the thickness of the adsorbent bed would increase, intra-grain diffusion might limit the adsorption process.^[43,44] Then, an additional model for the intragrain diffusion becomes necessary, which can easily be implemented due to the object-oriented modeling approach.^[13]

The sample carrier temperature T_{car} and the vapor temperature T_v are used as inputs for the model of the IR-LTJ experiment. Then, for a given set of the effective heat transfer coefficients $U_{\text{sor-hx,eff}}$ and $k_{\text{sor,eff}}$ and the diffusion coefficient D_{eff} , the model returns the temporal evolution of the adsorbent top surface temperature $T_{\text{sor,top}}^{\text{sim}}$ and the pressure of the vapor phase p_v^{sim} . The heat transfer and diffusion coefficients $U_{\text{sor-hx,eff}}$, $k_{\text{sor,eff}}$, and D_{eff} are determined by least-square fitting of the measured and simulated adsorbent top surface temperature $T_{\text{sor,top}}^{\text{exp}}$ and $T_{\text{sor,top}}^{\text{sim}}$ and the measured and simulated vapor pressure p_v^{exp} and p_v^{sim} . For this purpose, we determine the root-mean-square deviation RMSD_p of the vapor pressure and the root-mean-square deviation RMSD_T of the adsorbent top surface temperature

$$\text{RMSD}_p(U_{\text{sor-hx,eff}}, k_{\text{sor,eff}}, D_{\text{eff}}) = \sqrt{\frac{\sum_n (p_v^{\text{exp}} - p_v^{\text{sim}})^2}{n}} \quad \text{and} \quad (7)$$

$$\text{RMSD}_T(U_{\text{sor-hx,eff}}, k_{\text{sor,eff}}, D_{\text{eff}}) = \sqrt{\frac{\sum_n (T_{\text{sor,top}}^{\text{exp}} - T_{\text{sor,top}}^{\text{sim}})^2}{n}} \quad (8)$$

Because we conduct experiments with two bed heights h_1 and h_2 , we receive two values each for RMSD_p and RMSD_T . To find

the optimal combination of $U_{\text{sor-hx,eff}}$, $k_{\text{sor,eff}}$, and D_{eff} , we determine the geometric mean RMSD of all four RMSDs. We use the geometric mean, because it is independent from scaling of the single RMSD values^[45]

$$\overline{\text{RMSD}} = \sqrt[4]{\text{RMSD}_p^{h_1} \cdot \text{RMSD}_T^{h_1} \cdot \text{RMSD}_p^{h_2} \cdot \text{RMSD}_T^{h_2}} \quad (9)$$

We conduct separate experiments and simulations for adsorption and desorption and, thus, receive heat transfer and diffusion coefficients for the adsorption and desorption.

2.2. Predicting the Performance of Adsorption Chillers

The heat transfer and diffusion coefficients $U_{\text{sor-hx,eff}}$, $k_{\text{sor,eff}}$, and D_{eff} are used to parametrize a full-scale adsorption chiller model. In this study, we choose a one-bed adsorption chiller, yet other cycle designs could also be implemented. The one-bed adsorption chiller model consists of models for the adsorber, the condenser, and the evaporator, and allows varying the temperatures and volume flows of adsorber ($\dot{V}_{\text{ads/des}}$ and $T_{\text{ads/des}}$), evaporator (\dot{V}_{evap} and T_{evap}), and condenser (\dot{V}_{cond} and T_{cond}), and the cycle times for adsorption and desorption τ_{ads} and τ_{des} .

We implement a model for a finned-tube adsorber (Figure 4a). The model of the adsorber allows varying the number of fins n_{fin} , the width of the fins b_{fin} , the height of the fins and the adsorbent

bed h_{bed} , the length, the inner diameter and the outer diameter of the adsorber tube l_{tube} , $d_{\text{tube,in}}$, $d_{\text{tube,out}}$, the material of the tube and fins, and the parameters of the adsorbent configuration. In addition to the bed height, we can vary the working pair, the bed density ρ_{bed} , the particle diameter d_{particle} , and the heat transfer and diffusion coefficients $U_{\text{sor-hx,eff}}^{\text{ads,des}}$, $k_{\text{sor,eff}}^{\text{ads,des}}$, and $D_{\text{eff}}^{\text{ads,des}}$ for adsorption and desorption. All parameters are shown in Table 1. To be able to vary the geometry of the finned-tube adsorber, we discretize the adsorber in tangential x , radial y , and longitudinal z_{bed} direction of the tube (Figure 4a). Other adsorber geometries, such as plate heat exchanger, could also be implemented.

The condenser and evaporator are implemented as lumped-parameter models, which were fitted to experimental data by Lanzerath.^[46] In the remainder of this section, we present the adsorber model (Section 2.2.1) and the adsorption chiller model in detail (Section 2.2.2).

2.2.1. Adsorber Model

In the model of the finned-tube adsorber, heat transfer occurs in the tube, fins, and adsorbent bed in three dimensions (tangential x , radial y , and longitudinal z_{bed}). We assume that the distribution of temperature and loading in the adsorbent bed is always symmetric between two fins (cf., Figure 4a). Thus, we need to

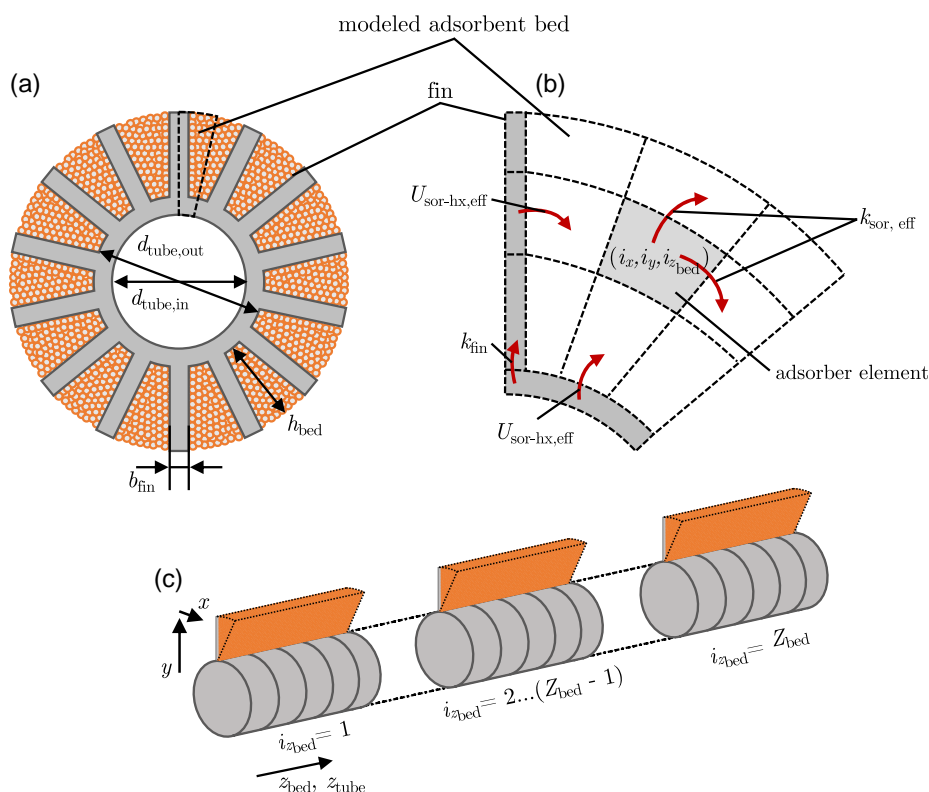


Figure 4. a) Profile of implemented adsorber geometry. Between two fins, the distribution of temperature and loading in the adsorbent bed is assumed always symmetric. Thus, only half of the adsorbent bed between two fins is modeled (indicated by dashed box). b) Detailed view of modeled fin and adsorbent bed with occurring heat flow rates. c) 3D view of discretized adsorber, indicating the dimensions of discretization in tangential x , radial y , and longitudinal z_{bed} and z_{tube} directions of the tube.

Table 1. Parameters of the distributed parameter adsorber model. The effective heat transfer and diffusion coefficients $U_{\text{sor-hx,eff}}^{\text{ads,des}}$, $k_{\text{sor,eff}}^{\text{ads,des}}$, and $D_{\text{eff}}^{\text{ads,des}}$ are determined from the IR-LTJ model (Section 2.1).

Material of the tube and the fins	
Number of the fins	n_{fin}
Width of the fins	b_{fin}
Height of the fins and the adsorbent bed	h_{bed}
Length of the adsorber tube	l_{tube}
Inner diameter of the adsorber tube	$d_{\text{tube,in}}$
Outer diameter of the adsorber tube	$d_{\text{tube,out}}$
Working pair	
Bed density	ρ_{bed}
Particle diameter	d_{particle}
Effective heat transfer coefficient between heat	$U_{\text{ads,des}}^{\text{ads,des}}$
Exchanger and adsorbent bed configuration	
Effective heat conductivity in	$k_{\text{sor,eff}}^{\text{ads,des}}$
Adsorbent bed configuration	
Effective diffusion coefficient	$D_{\text{eff}}^{\text{ads,des}}$

model only half a fin and half of the adsorbent bed between two fins and scale up the resulting heat and mass flow rates by two times the number of fins $2n_{\text{fin}}$.

Similar to Section 2.1, we describe 3D heat transfer in the fin and the adsorbent bed by partial differential equations. The energy balance of the fin reads^[47]

$$\rho_{\text{fin}} c_{\text{fin}} \frac{\partial T_{\text{fin}}}{\partial t} = k_{\text{fin}} \nabla^2 T_{\text{fin}} \quad (10)$$

with the density ρ_{fin} and the specific heat capacity c_{fin} of the fin material, the temperature of a fin element T_{fin} , the thermal conductivity k_{fin} within the fin, and the nabla operator ∇ .

The first boundary condition comes from the thermal connection of the fin to the tube at $y = 0$ and the outer radius of the tube $r = R$ (cf., Figure 4c)

$$k_{\text{fin}} \frac{\partial T_{\text{fin}}}{\partial y} \Big|_{y=0} = k_{\text{tube}} \frac{\partial T_{\text{tube}}}{\partial r} \Big|_{r=R} \quad (11)$$

with the discretization of the tube in radial direction r . In this study, tube and fins are both made from the same material, leading to the same thermal conductivity $k_{\text{fin}} = k_{\text{tube}}$. The second boundary condition comes from thermal connection of the fin to the adsorbent bed at $x = b_{\text{fin}}/2$

$$k_{\text{fin}} \frac{\partial T_{\text{fin}}}{\partial x} \Big|_{x=b_{\text{fin}}/2} = U_{\text{sor-hx,eff}} (T_{\text{sor}} - T_{\text{fin}}) \Big|_{x=b_{\text{fin}}/2} \quad (12)$$

The energy balance of the adsorbent bed is the same as for the IR-LTJ adsorbent (cf., Equation (1)), but with 3D heat transfer^[34]

$$\underbrace{\rho_{\text{sor}} (c_{\text{sor}} + c_{\text{ad}} w) \frac{\partial T_{\text{sor}}}{\partial t}}_1 + \underbrace{\rho_{\text{sor}} u_{\text{ad}} \frac{\partial w}{\partial t}}_2 = \underbrace{k_{\text{sor,eff}} \nabla^2 T_{\text{sor}}}_3 + \underbrace{\rho_{\text{sor}} h_v \frac{\partial w}{\partial t}}_4 \quad (13)$$

with 1) the change in internal energy from change in temperature $\frac{\partial T_{\text{sor}}}{\partial t}$ with the specific heat capacity of the dry adsorbent c_{sor} and the adsorbed phase c_{ad} , and the loading w ; 2) the change in internal energy from change in loading $\frac{\partial w}{\partial t}$ with the specific internal energy of the adsorbed phase u_{ad} ; 3) 3D heat flow due to the thermal conduction in the adsorbent bed with the thermal conductivity $k_{\text{sor,eff}}$ within the adsorbent bed and the nabla operator ∇ ; 4) the enthalpy flow rate of the adsorbate $\rho_{\text{sor}} h_v \frac{\partial w}{\partial t}$.

The mass balance of the adsorbent bed is also the same as for the mass balance of the IR-LTJ adsorbent bed element (Equation (3)).

The boundary conditions come from thermal connection of the adsorbent bed to the fins and the tube

$$k_{\text{sor,eff}} \frac{\partial T_{\text{sor}}}{\partial x} \Big|_{x=b_{\text{fin}}/2} = U_{\text{sor-hx,eff}} (T_{\text{fin}} - T_{\text{sor}}) \Big|_{x=b_{\text{fin}}/2} \quad \text{and} \quad (14)$$

$$k_{\text{sor,eff}} \frac{\partial T_{\text{sor}}}{\partial y} \Big|_{y=0} = U_{\text{sor-hx,eff}} (T_{\text{tube}} - T_{\text{sor}}) \Big|_{y=0} \quad (15)$$

Similar to the IR-LTJ modeling, we need to discretize the partial differential equations in space for use in Modelica. Again, the resulting equations correspond to models for the adsorbent and heat and mass transfer (Figure 5), which is identical to the models used in the IR-LTJ model (cf., Section 2.1). Furthermore, we added a model for the tube. The tube model is taken from the TIL library provided by TLK-Thermo GmbH.^[38] The tube model accounts for the geometry and the resulting heat capacity of the tube and is discretized in longitudinal direction z_{tube} , as mentioned previously. The heat transfer inside the tube is determined by the correlation of Sieder and Tate.^[48] The finally implemented model equations in Modelica can be found in the Supporting Information.

The adsorber is discretized in tangential x , radial y , and longitudinal direction z of the tube (with X , Y , and Z as total numbers of discrete elements). The temperature of the adsorbent bed varies only slightly in longitudinal direction compared with radial and tangential direction. Thus, a fine discretization of the adsorbent bed in longitudinal direction is not necessary. However, a fine discretization in longitudinal direction is necessary for the tube to accurately model the fluid flow in the tube.^[46,49] Therefore, to reduce the number of differential states, we apply different levels of discretization for the adsorbent bed Z_{bed} and the tube Z_{tube} .

To determine the pressure drop in the full-scale adsorber, we use the same approach as in Section 2.1. In the full-scale adsorber, the cross-sectional area becomes $A_{\text{car}} = 0.013 \text{ m}^2$ and the mean distance is $\delta y = 3.74 \text{ mm}$. The vapor density $\rho_v = 0.94 \times 10^{-3} \text{ kg m}^{-3}$, the dynamic viscosity $\eta = 9.24 \times 10^{-6} \text{ Pa s}$, and the mass flow $\dot{m}_{\text{ad}} = 3.73 \times 10^{-5} \text{ kg s}^{-1}$ are taken from simulations of the adsorption phase of the case study (cf., Section 3.3), resulting in a maximum pressure drop of 28.4 Pa. Compared with the absolute pressure,

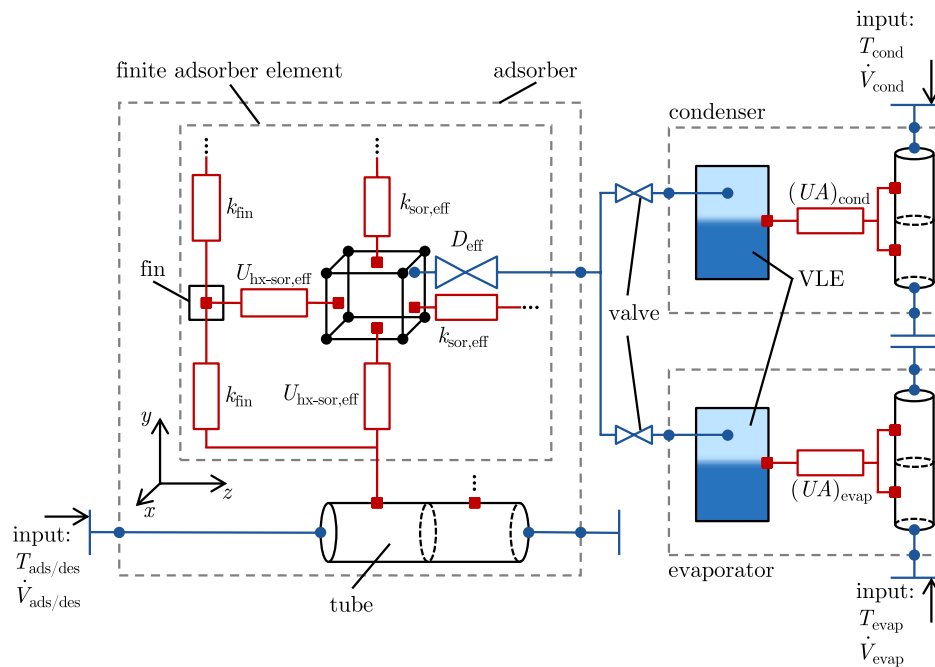


Figure 5. Dynamic model of full-scale adsorption chiller. The adsorber consists of models for the adsorbent, the fin, and the tube, connected by heat transfer models. The adsorber model is connected to models of the evaporator and condenser via a mass transfer model and valve models. The evaporator and condenser models consist of models for the VLE and tubes, connected with heat transfer models. The adsorber is discretized in tangential x , radial y , and longitudinal z_{bed} and z_{tube} directions of the tube (with X , Y , Z_{bed} , and Z_{tube} as the total numbers of discrete elements), whereas the evaporator and the condenser are discretized in longitudinal directions l_{evap} and l_{cond} of the evaporator/condenser tube.

the pressure drop is 2% and thus is negligible. Because the pressure drop is negligible, we connected all adsorbent elements directly to the vapor phase of the condenser or the evaporator (Figure 5).

2.2.2. Adsorption Chiller Model

The adsorber model described in Section 2.2.1 is connected to models of the evaporator and the condenser (Figure 5) to model the full-scale one-bed adsorption chiller. The evaporator and condenser models are taken from SorpLib.^[10] The evaporator and condenser models are identical, differing only in parametrization of the geometry and the heat transfer coefficient. The evaporator and condenser are connected via valve models to the adsorber. The valve models are implemented to control the vapor flow during the adsorption and desorption phase, without leading to any pressure losses. The evaporator/condenser model consists of models for the heat exchanger tube, vapor–liquid equilibrium (VLE), and the heat transfer between the tube and the vapor–liquid phase (Figure 5).

In the VLE model, the adsorptive is assumed to be in a two-phase region, with the vapor phase being saturated $p_{evap/cond} = p_{sat}(T_{evap/cond})$ and the temperature to be homogeneous $T_{evap/cond}$. The volume is defined constant $V_{evap/cond}$ and the mass balance is described by

$$\frac{dm_{evap/cond,ad}}{dt} = V_{evap/cond} \frac{d\rho_{evap/cond,ad}}{dt} = \dot{m}_{ad} \quad (16)$$

with the mass of adsorptive $m_{evap/cond,ad}$ in the constant volume $V_{evap/cond}$, the density $\rho_{evap/cond,ad}$, and the resulting adsorptive mass flow \dot{m}_{ad} .

The energy balance reads

$$\frac{dU_{evap/cond,ad}}{dt} = \dot{m}_{ad}h_{ad} + \dot{Q}_{evap/cond} \quad (17)$$

The change of internal energy $\frac{dU_{evap/cond,ad}}{dt}$ results from the adsorptive enthalpy flow $\dot{m}_{ad}h_{ad}$ and the heat flow rate from/to the tube $\dot{Q}_{evap/cond}$. The specific enthalpy h_{ad} depends on the direction of the mass flow \dot{m}_{ad} . During adsorption, the adsorptive is evaporated in the evaporator and flows to the adsorber with the saturated specific enthalpy $h_{ad}(T_{evap})$. During desorption, the adsorptive flows from the adsorber with the specific enthalpy $h_{ad}(T_{ads}, p_{cond})$ to the condenser and is condensed. Details of the VLE model can be found in Bau et al.^[10]

The tube model is taken from the TIL library and is discretized in longitudinal flow direction with L as total number of discrete elements. The VLE model and the discretized tube are connected via a heat transfer model

$$\dot{Q}_{evap/cond} = \frac{(UA)_{evap/cond}}{L} \sum_{i=1}^L (T_{tube,i} - T_{evap/cond}) \quad (18)$$

with the heat transfer coefficient $(UA)_{evap/cond}$ of the condenser or the evaporator.

The adsorption chiller model simulates the heat flow rates in adsorber, condenser, and evaporator. The heat flow rates are used to calculate the COP and the SCP of the adsorption chiller, with the cycle time $\Delta\tau_{\text{cycle}}$

$$\text{COP} = \frac{\int_0^{\tau_{\text{ads}}} \dot{Q}_{\text{evap}} dt}{\int_0^{\tau_{\text{ads}}} \dot{Q}_{\text{ads}} dt} \text{ and} \quad (19)$$

$$\text{SCP} = \frac{\int_0^{\tau_{\text{ads}}} \dot{Q}_{\text{evap}} dt}{m_{\text{sor}} \cdot \tau_{\text{cycle}}} \quad (20)$$

with the adsorption time τ_{ads} , the desorption time τ_{des} , and the cycle time τ_{cycle} as sum of the times for adsorption τ_{ads} and desorption τ_{des}

$$\tau_{\text{cycle}} = \tau_{\text{ads}} + \tau_{\text{des}} \quad (21)$$

The times for isosteric heating and cooling are implicitly included in the desorption time τ_{des} and the adsorption time τ_{ads} , respectively. The times for isosteric heating and isosteric cooling directly depend on the pressure in the condenser and evaporator: isosteric heating stops when the pressure in the adsorber becomes higher than in the condenser, and isosteric cooling stops when the pressure in the adsorber becomes lower than in the evaporator.

The coefficients for the heat transfer between the tube and the adsorbent bed configuration $U_{\text{sor-hx,eff}}$, the effective heat conductivity in the adsorbent bed configuration $k_{\text{sor,eff}}$, and the effective overall diffusion coefficient D_{eff} are taken from the small-scale IR-LTJ experiment discussed in Section 2.1.

3. Case Study: Predicting the Performance of a One-Bed Adsorption Chiller

In this section, we present a case study in which we determine the heat transfer and diffusion coefficients of a packed-bed adsorbent configuration with the working pair silica gel 123/water from IR-LTJ experiments (Section 3.1). The heat transfer and diffusion coefficients are used to parametrize the adsorption chiller model, combined with geometric information of a real adsorption chiller (Section 3.2). We predict the heat flows in the adsorber and both the power density SCP and COP for different

cycle times and process temperatures, and compare the results with experiments of a full-scale adsorption chiller (Section 3.3).

3.1. Heat Transfer and Diffusion Coefficients from the Extended Small-Scale IR-LTJ Experiment

In the case study, we investigate the working pair silica gel 123/water^[50] with a mean particle size of $d_{\text{particle}} = 0.9 \text{ mm}$ and a packed-bed density of $\rho_{\text{bed}} = 635 \text{ kg m}^{-3}$. We place the adsorbent on a sample carrier made from aluminum, the same material as the full-scale heat exchanger in the adsorber. We conduct separate IR-LTJ experiments with an evaporation temperature $T_{\text{evap}} = 10^\circ$, an adsorption and condensation temperature of $T_{\text{ads}} = T_{\text{cond}} = 30^\circ$ and a desorption temperature of $T_{\text{des}} = 80^\circ$, resulting in the calibration temperature set of $10/30/80^\circ\text{C}$. We perform experiments for the bed heights $h_{\text{bed}} = 1 \text{ mm}$ and 2 mm each for adsorption and desorption. The results for the adsorption experiments are shown in Figure 6a for a bed height of 1 mm and in Figure 6b with a bed height of 2 mm . Both the pressure p_v and the top-surface temperature of the adsorbent $T_{\text{sor,top}}$ follow the sample carrier temperature T_{car} .

We use the experimental data to calibrate the heat transfer and diffusion coefficients $U_{\text{sor-hx,eff}}$, $k_{\text{sor,eff}}$, and D_{eff} in the IR-LTJ model (cf., Section 2.1). For this purpose, we simulate the adsorption and desorption process for different combinations of the heat transfer and diffusion coefficients. For each combination, the root-mean-square deviation RMSD is determined (cf., Equation (9)) and shown in Figure 7.

The figure shows a distinct minimum of the $\overline{\text{RMSD}}$ for the thermal conductivity $k_{\text{sor,eff}}^{\text{ads}}$ and the diffusion coefficient $D_{\text{eff}}^{\text{ads}}$. For a thermal conductivity of $0.22 \text{ W m}^{-1} \text{ K}^{-1}$ and a diffusion coefficient of $1.3 \times 10^{-9} \text{ m}^2 \text{ s}^{-1}$, $\overline{\text{RMSD}}$ becomes minimal. For the heat transfer coefficient $U_{\text{sor-hx,eff}}^{\text{ads}}$, a distinct optimal value cannot be determined. In the IR-LTJ experiments, the heat transfer between adsorbent and heat exchanger is only limiting for values smaller than $U_{\text{sor-hx,eff}}^{\text{ads}} = 430 \text{ W m}^{-2} \text{ K}^{-1}$. For a larger heat transfer coefficient, the thermal conductivity $k_{\text{sor,eff}}^{\text{ads}}$ is limiting the heat transfer in the IR-LTJ experiments. Even though we perform two experiments with different bed heights, the information drawn from the experiments is not sufficient to

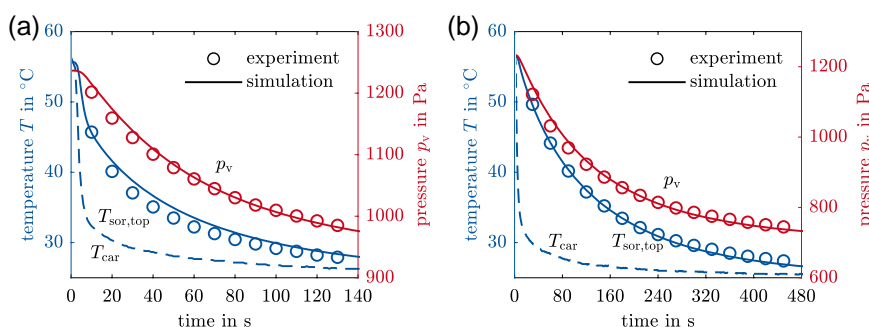


Figure 6. Measured pressure of vapor phase p_v , top surface temperature of the adsorbent $T_{\text{sor,top}}$, and sample carrier temperature T_{car} for adsorption experiments, and a) bed height $h = 1 \text{ mm}$ and b) bed height $h = 2 \text{ mm}$ in IR-LTJ setup. In addition, the fitted pressure and adsorbent temperature are shown for the heat transfer and diffusion coefficients $U_{\text{sor-hx,eff}}^{\text{ads}} = 430 \text{ W m}^{-2} \text{ K}^{-1}$, $k_{\text{sor,eff}}^{\text{ads}} = 0.22 \text{ W m}^{-1} \text{ K}^{-1}$, and $D_{\text{eff}}^{\text{ads}} = 1.3 \times 10^{-9} \text{ m}^2 \text{ s}^{-1}$ (cf., Table 2).

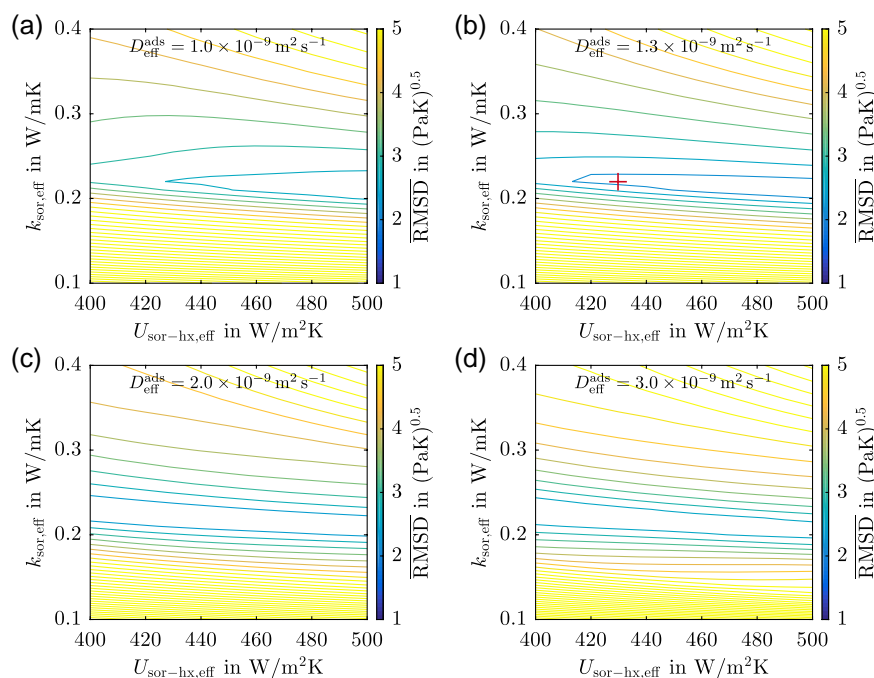


Figure 7. Root-mean-square deviation $\overline{\text{RMSD}}$ (cf., Equation (22)) for the adsorption experiment as a function of the heat transfer coefficient $U_{\text{sor-hx,eff}}^{\text{ads}}$, the thermal conductivity $k_{\text{sor,eff}}^{\text{ads}}$, and the diffusion coefficient $D_{\text{eff}}^{\text{ads}}$: a) $D_{\text{eff}}^{\text{ads}} = 1.0 \times 10^{-9} \text{ m}^2 \text{ s}^{-1}$, b) $D_{\text{eff}}^{\text{ads}} = 1.3 \times 10^{-9} \text{ m}^2 \text{ s}^{-1}$, c) $D_{\text{eff}}^{\text{ads}} = 2.0 \times 10^{-9} \text{ m}^2 \text{ s}^{-1}$, d) $D_{\text{eff}}^{\text{ads}} = 3.0 \times 10^{-9} \text{ m}^2 \text{ s}^{-1}$. The parameter set marked with “+” is used for further investigation.

determine a distinct value heat transfer coefficient $U_{\text{sor-hx,eff}}^{\text{ads}}$. In particular, the adsorbent bed heights of $h_{\text{bed}} = 1$ and 2 mm might be too close to each other. We choose a value for the heat transfer coefficient ($U_{\text{sor-hx,eff}}^{\text{ads}} = 430 \text{ W m}^{-2} \text{ K}^{-1}$) with a low $\overline{\text{RMSD}}$ value. For the heat transfer coefficient $U_{\text{sor-hx,eff}}^{\text{ads}} = 430 \text{ W m}^{-2} \text{ K}^{-1}$, the thermal conductivity of $k_{\text{sor,eff}}^{\text{ads}} = 0.22 \text{ W m}^{-1} \text{ K}^{-1}$, and the diffusion coefficient $D_{\text{eff}}^{\text{ads}} = 1.3 \times 10^{-9} \text{ m}^2 \text{ s}^{-1}$, $\overline{\text{RMSD}}$ becomes $2.0(\text{PaK})^{0.5}$.

While applying the measurement uncertainty of the adsorbent temperature $u_{\text{IR}} = 0.11 \text{ K}$ for RMSD_T and the measurement uncertainty of the pressure sensor $u_p = 5.78 \text{ Pa}$ for RMSD_p in Equation (9), we obtain an $\overline{\text{RMSD}}$ value of $0.8(\text{PaK})^{0.5}$. The fitted heat transfer and diffusion coefficients lead to a 1.5 higher $\overline{\text{RMSD}}$. The accuracy is shown to be sufficient by the validation experiments in Section 3.3. The main deviations are found for the smaller bed size suggesting that the steeper gradients cannot be fully resolved by the model (Figure 6a). Still, the diffusion coefficient of $D_{\text{eff}}^{\text{ads}} = 1.3 \times 10^{-9} \text{ m}^2 \text{ s}^{-1}$ is in line with the previous findings. In a former study, we determined a mean diffusion coefficient of $1.410^{-9} \text{ m}^2 \text{ s}^{-1}$ for the similar working pair Siogel/water.^[32] Also, Gurgel et al.^[51] determined a diffusion coefficient of $1.9 \times 10^{-9} \text{ m}^2 \text{ s}^{-1}$ for silica gel/water, which is the same magnitude as our determined value.

Also, our value for thermal conductivity $k_{\text{sor,eff}}^{\text{ads}}$ is in line with the literature: values range from 0.05 to $0.2 \text{ W m}^{-1} \text{ K}^{-1}$ ^[52,53] for a packed-bed configuration and up to $1.2 \text{ W m}^{-2} \text{ K}^{-1}$ for the thermal conductivity in the adsorbent grain^[34] of silica gel/water.

The heat transfer coefficient of $U_{\text{sor-hx,eff}}^{\text{ads}} = 430 \text{ W m}^{-2} \text{ K}^{-1}$ is considerably larger than the values from the literature with 120 ^[54] and $280 \text{ W m}^{-2} \text{ K}^{-1}$.^[55] However, in the mentioned studies, the heat transfer coefficient $U_{\text{sor-hx,eff}}$ also includes the thermal conductivity in the adsorbent bed; thus, the literature values are expected to be smaller than the values found here.

The results for desorption are very similar. The corresponding figures for desorption can be found in the Supporting Information. For desorption, we identified values for the thermal conductivity $k_{\text{sor,eff}}$ of $0.35 \text{ W m}^{-1} \text{ K}^{-1}$, for the heat transfer coefficient $U_{\text{sor-hx,eff}}$ of $660 \text{ W m}^{-2} \text{ K}^{-1}$, and for the diffusion coefficient D_{eff} of $1.4 \times 10^{-9} \text{ m}^2 \text{ s}^{-1}$. For desorption, all determined heat transfer and diffusion coefficients are higher than the coefficients for adsorption. The higher coefficients indicate the faster kinetics of desorption due to higher pressures and temperatures.^[56] All heat transfer and diffusion coefficients are shown in Table 2.

Table 2. Effective heat transfer and diffusion coefficients $U_{\text{sor-hx,eff}}$, $k_{\text{sor,eff}}$, and D_{eff} (cf., Figure 2) determined from the IR-LT method (cf., Section 2.1) for a loose-grain configuration of silica gel 123 (mean particle size 0.9 mm) and the temperature set of $10/30/80^\circ \text{C}$. The coefficients are in line with the findings from the literature.

	$U_{\text{sor-hx,eff}} [\text{W m}^{-2} \text{ K}^{-1}]$	$k_{\text{sor,eff}} [\text{W m}^{-1} \text{ K}^{-1}]$	$D_{\text{eff}} [\text{m}^2 \text{ s}^{-1}]$
Adsorption	430	0.22	1.3×10^{-9}
Desorption	660	0.35	1.4×10^{-9}

3.2. Parametrization of the Full-Scale Adsorption Chiller Model

We parametrize the adsorption chiller model with the geometric information of a prototype full-scale one-bed adsorption chiller, constructed by Lanzerath^[46] (Figure 8a). The adsorption chiller consists of a modular adsorber, a condenser, and an evaporator, and was evaluated experimentally in a test bench. The test bench allows varying the temperatures and the cycle times. We measure the heat flow rates of the adsorber, the evaporator, and the condenser, from which the SCP and the COP are determined (cf., Equation (19) and (20)).

For the condenser and evaporator models, the geometry parameters and heat transfer coefficients have been taken from Lanzerath.^[46] All parameters of the adsorption chiller model are shown in Table 3. To parametrize the heat and mass transfer models in the adsorber, we use the previously determined heat transfer and diffusion coefficients in the adsorber $U_{\text{sor-hx,eff}}$, $k_{\text{sor,eff}}$, and D_{eff} (Table 2).

We modeled the adsorber for perfectly orthogonal fins around the tube (cf., Figure 4). However, in the real adsorber geometry for validation, the fins are not vertically aligned on the tube, but are curved (Figure 8b). The curved fins lead to a higher contact

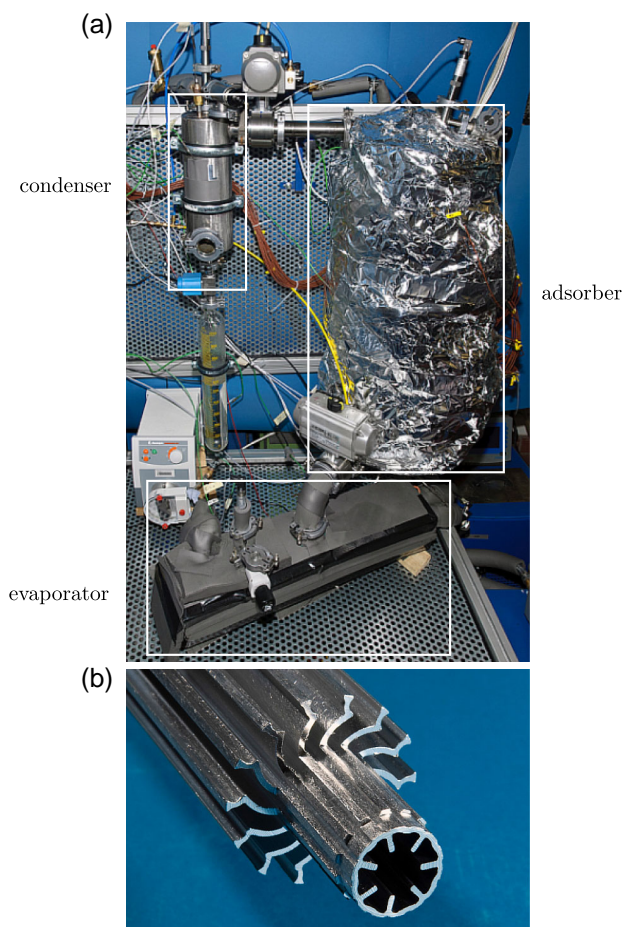


Figure 8. a) Experimental setup of full-scale adsorption chiller in one-bed configuration, consisting of adsorber, condenser, and evaporator, constructed by Lanzerath.^[46] b) Fin structure of adsorber tubes.

Table 3. Parametrization of the full-scale adsorption chiller model. Parameters of the adsorber model are taken from Lanzerath^[46] and Bau.^[49] The parameters $A_{\text{fin,bed}}$, V_{bed} , and V_{bed} were separately calculated from the real adsorber geometry with data from Bau.^[49] Parameters of the condenser and evaporator model are taken from Lanzerath.^[46]

Parameters of the adsorber model			
Material of the tube and the fins		Aluminum	
Number of the fins	n_{fin}	14	
Width of the fins	b_{fin}	1.42	mm
Height of the fins and the adsorbent bed	h_{bed}	9.85	mm
Length of the adsorber tube	l_{tube}	7.355	m
Inner diameter of the adsorber tube	$d_{\text{tube,in}}$	12.85	mm
Outer diameter of the adsorber tube	$d_{\text{tube,out}}$	15.71	mm
Heat transfer inside the tube	$(UA)_{\text{hx-fluid,ads}}$	Sieder and Tate ^[48]	
Sieder parameter	C_{Sieder}	0.033885	
Working pair		Silica gel 123/water ^[50]	
Bed density	ρ_{bed}	761.49	Kg m ⁻³
Particle diameter	d_{particle}	0.9	mm
Separately calculated geometric parameters of the adsorber model			
Volume of the adsorbent bed	V_{bed}	0.0031	m ³
Area between adsorbent bed and tube	$A_{\text{tube,bed}}$	0.012	m ²
Area between fins and adsorbent	$A_{\text{fin,bed}}$	1.653	m ²
Parameters of the condenser model			
Material of the tube		Copper	
Length of the condenser tube	l_{cond}	4.55	m
Inner diameter of the condenser tube	$d_{\text{cond,in}}$	8.0	mm
Outer diameter of the condenser tube	$d_{\text{cond,out}}$	10.0	mm
Heat transfer inside the tube	$(UA)_{\text{hx-fluid,cond}}$	Schmidt ^[57]	
Heat transfer outside the tube	$(UA)_{\text{cond,out}}$	3174	W K ⁻¹
Parameters of the evaporator model			
Material of the tube		Copper	
Length of the evaporator tube	l_{evap}	2.31	m
Inner diameter of the evaporator tube	$d_{\text{evap,in}}$	14.67	mm
Outer diameter of the evaporator tube	$d_{\text{evap,out}}$	17.72	mm
Heat transfer inside the tube	$(UA)_{\text{hx-fluid,evap}}$	Sieder and Tate ^[48]	
Sieder parameter	C_{Sieder}	0.05	
Heat transfer outside the tube	$(UA)_{\text{evap,out}}$	176	W K ⁻¹

area $A_{\text{fin,bed}}$ between the fins and the adsorbent, but reduce the volume of the adsorbent bed V_{bed} . In addition, the area between the adsorbent bed and the tube $A_{\text{tube,bed}}$ is reduced. To account for the different areas and volumes, we, therefore, calculate the parameters $A_{\text{fin,bed}}$, V_{bed} , and V_{bed} from the real adsorber geometry with data from Bau.^[49]

We identify the number of discretization elements in tangential, radial, and longitudinal direction of the adsorber to $X = 8$, $Y = 6$, $Z_{\text{bed}} = 10$, and $Z_{\text{tube}} = 40$, respectively, as a compromise between modeling accuracy and computational time (cf., Supporting Information). For the evaporator and the condenser tubes, we choose the same number of discretization

elements as in Lanzerath,^[46] namely $L_{\text{evap}} = L_{\text{cond}} = 10$ for both the evaporator and the condenser tubes.

3.3. Predicting the Performance with the Full-Scale Adsorption Chiller Model

With the parametrized model for the full-scale adsorption chiller, we predict the heat flow rates in the adsorber, condenser, and evaporator. For this purpose, we perform a simulation for an evaporation temperature of $T_{\text{evap}} = 10^\circ\text{C}$, an adsorption and condensation temperature of $T_{\text{ads/cond}} = 35^\circ\text{C}$, and a desorption temperature of $T_{\text{des}} = 90^\circ\text{C}$. The temperatures differ slightly from the temperature set of 10/30/80 °C used for the IR-LTJ experiments (cf., Section 3.1). However, in a former study, we showed that the determined heat transfer and diffusion coefficients are also valid for temperature ± 10 K of the calibration temperature set.^[31] Thus, a recalibration of the heat transfer and diffusion coefficients is not necessary for the temperature set of the full-scale adsorption chiller. We set the cycle times for the adsorption and desorption to $\tau_{\text{ads/des}} = 900$ s.

In **Figure 9**, the resulting heat flow rates in the adsorber are shown for the adsorption phase (Figure 9a) and the desorption phase (Figure 9b). Compared with the measured heat flow rate in the test bench, the prediction shows excellent agreement. The peak at the beginning of adsorption and desorption is matched with high accuracy. Hereafter, the predicted heat flow rate is slightly underestimated compared with the experiment. Lanzerath^[46] obtained the same deviation for his fitted model and explained the underestimation from the discretization of the adsorber tube and the inertia of the volume flow sensor.

Both effects lead to a faster decrease in the simulated heat flow rate.

We measure the accuracy of the predicted heat flow rate in the adsorber $\dot{Q}_{\text{ads}}^{\text{pred}}$ by means of the root-mean-square deviation $\text{RMSD}_{\dot{Q}_{\text{ads}}}$ and the coefficient of variation $\text{CV}(\text{RMSD}_{\dot{Q}_{\text{ads}}})$

$$\text{RMSD}_{\dot{Q}_{\text{ads}}} = \sqrt{\frac{\int_0^{\tau_{\text{cycle}}} (\dot{Q}_{\text{ads}}^{\text{exp}} - \dot{Q}_{\text{ads}}^{\text{pred}})^2 dt}{\tau_{\text{cycle}}}} \quad (22)$$

$$\text{CV}(\text{RMSD}_{\dot{Q}_{\text{ads}}}) = \frac{\text{RMSD}}{\int_0^{\tau_{\text{cycle}}} \dot{Q}_{\text{ads}}^{\text{exp}} dt / \tau_{\text{cycle}}} \quad (23)$$

with the measured heat flow rate in the adsorber $\dot{Q}_{\text{ads}}^{\text{exp}}$ and the cycle time τ_{cycle} (cf., Equation (21)).

For the previously discussed experiment, we determine a CV of 12.5%. The CV is even slightly better than in Lanzerath,^[46] who also simulated the full-scale adsorption chiller and determined a CV of 14.0%. Noteworthy, Lanzerath calibrated the heat transfer and diffusion coefficients directly to the full-scale adsorption chiller experiment. In contrast, in this study, the heat transfer and diffusion coefficients are determined from the small-scale IR-LTJ experiment.

From the predicted heat flow rates, the power density SCP and the COP can be computed here to 84.4 W kg^{-1} and 0.36, respectively. Compared with the experimental power density SCP with 87.1 W kg^{-1} and COP with 0.35, the deviations are 3.1% and 2.4%. Thus, the deviations are considerably lower than the measurement uncertainties of 7.5% and 10.8%. Also, the predicted power density SCP and COP are in the same range as the

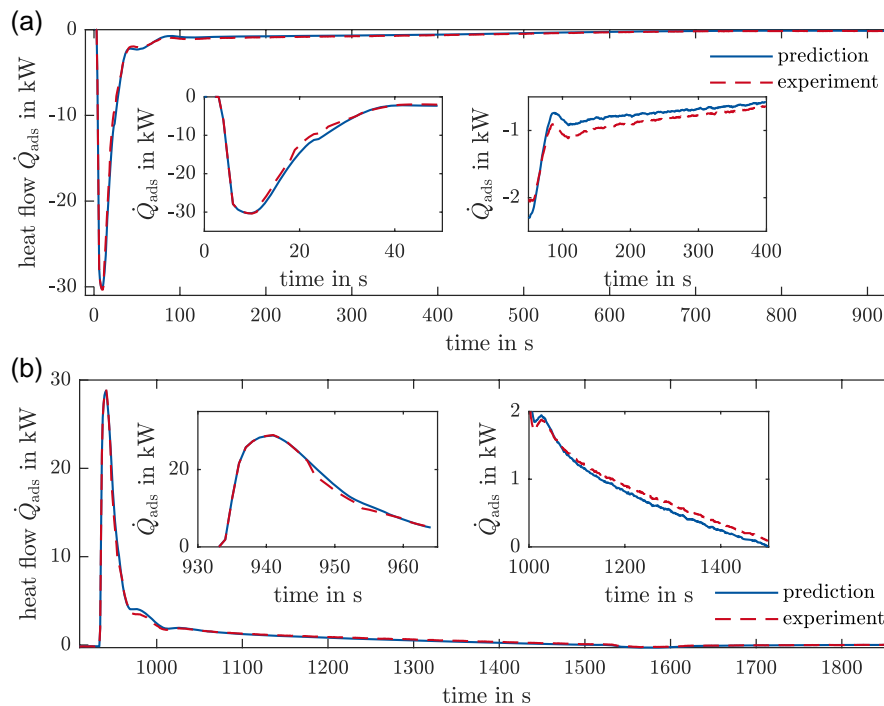


Figure 9. Predicted heat flow rates of adsorber during a) adsorption and b) desorption from the adsorption chiller model and heat flow rates from the experiment by Lanzerath^[46] for temperature set of 10/35/90 °C and cycle times $\tau_{\text{ads/des}} = 900$ s. In addition, shown are the zooms of the heat flow rates at the beginning and in the middle of the adsorption and desorption phases.

Table 4. Varied temperatures for evaporation T_{evap} , adsorption and condensation $T_{\text{ads/cond}}$, and for desorption T_{des} , as well as varied cycle time for adsorption and desorption $\tau_{\text{ads/des}}$ in full-scale adsorption chiller model. Changed parameters from reference case in first row are marked in bold.

T_{evap} [°C]	$T_{\text{ads/cond}}$ [°C]	T_{des} [°C]	$\tau_{\text{ads/des}}$ [s]
10	35	90	900
10	35	90	450
10	35	90	1800
5	35	90	900
20	35	90	900
10	35	70	900
10	35	110	900
10	25	90	900
10	45	90	900

simulated $\text{SCP} = 84.9 \text{ W kg}^{-1}$ and $\text{COP} = 0.35$ from the fitted model by Lanzerath.^[46]

Apart from the discussed case, we predict heat flows, the power density SCP, and the COP for other times for the adsorption and desorption $\tau_{\text{ads/des}}$, and temperatures of evaporation T_{evap} , adsorption and condensation $T_{\text{ads/cond}}$, and desorption T_{des} . The variations are shown in **Table 4**.

The prediction results are shown in **Figure 10** and compared with the fitted model of Lanzerath^[46] and to the experiment. In **Figure 10a**, the resulting $\text{CV}(\text{RMSD}_{\dot{Q}_{\text{ads}}})$ are shown. For most variations, the CV is lower than 20% and in the same range as the CV determined by Lanzerath. In addition, the power density SCP (**Figure 10b**) and the COP (**Figure 10c**) are predicted with high accuracy for all cases, with deviations mostly within the measurement uncertainties of the power density SCP and the COP.

Also, compared with other studies, the presented model predicts the power density SCP and COP with high accuracy

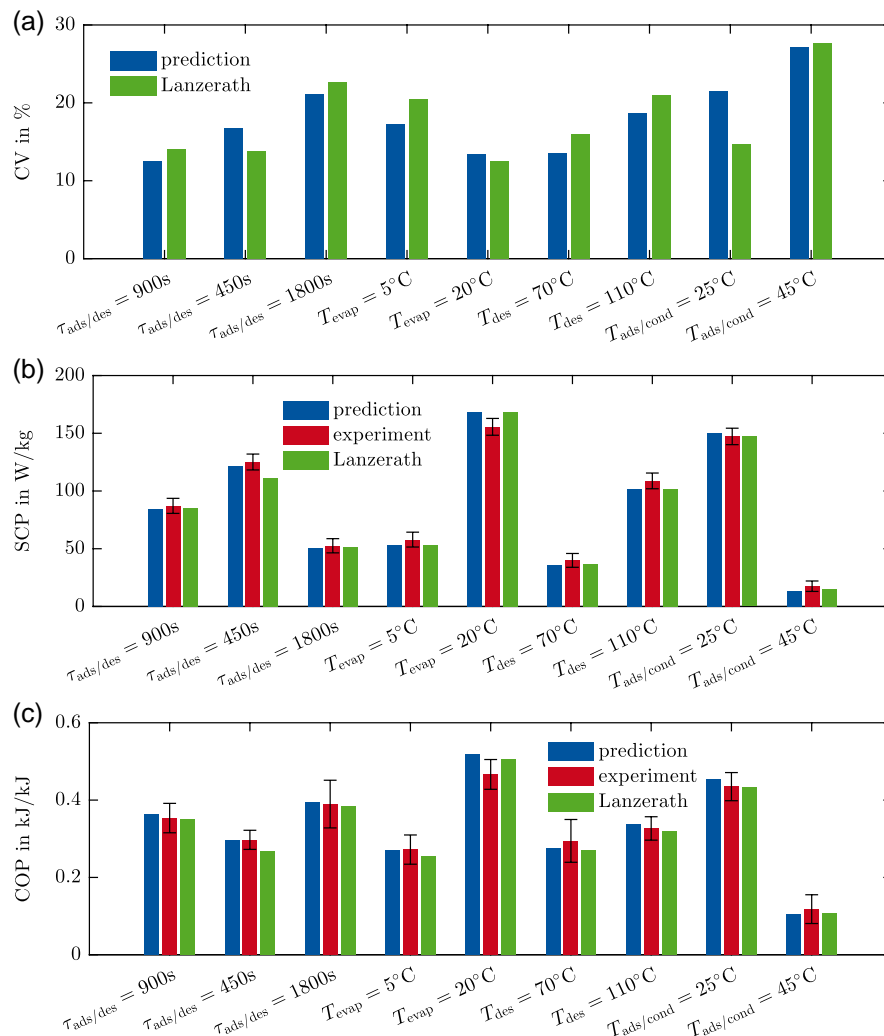


Figure 10. Prediction results for variations of the times for adsorption and desorption $\tau_{\text{ads/des}}$, the evaporation temperature T_{evap} , the desorption temperature T_{des} , and the adsorption and condensation temperature $T_{\text{ads/cond}}$ (cf., Table 4). a) Predicted $\text{CV}(\text{RMSD}_{\dot{Q}_{\text{ads}}})$ (Equation (23)) and CV determined by Lanzerath.^[46] b) Power density SCP and c) COP from prediction, experiment, and simulation by Lanzerath.^[46] Also indicated are the measurement uncertainties of the experiment.

achieved previously only by fitting. Schicktanztanz and Núñez^[16] and Wang et al.^[17] chose a similar modeling approach as Lanzerath^[46] and determined the SCP and COP with deviations between the simulated and measured SCP of around 5% and 7.5% and for the COP of around 6% and 12%, respectively.

In some cases (Figure 10; $\tau_{\text{ads/des}} = 900$ s, $\tau_{\text{ads/des}} = 1800$ s, $T_{\text{evap}} = 5^\circ$, $T_{\text{des}} = 70^\circ$, $T_{\text{des}} = 110^\circ$, $T_{\text{ads/cond}} = 45^\circ$), the predicted CV is even smaller than the CV determined by Lanzerath.^[46] Differences between the modeling approaches come only from the discretization of the adsorber bed and different heat transfer and diffusion coefficients. We determined the heat transfer and diffusion coefficients from the extended IR-LTJ experiments; Lanzerath calibrated the heat transfer and diffusion coefficients directly to the full-scale adsorption chiller experiment for the reference case ($\tau_{\text{ads/des}} = 900$ s). In the mentioned cases, our determined heat transfer and diffusion coefficients seem to better describe the experiments than the coefficients determined by Lanzerath. However, in other cases, Lanzerath's coefficients lead to smaller CV values and the deviations are not clearly systematic. Still, the deviations between experiment and simulation for the CV, the SCP, and the COP follow the same trends for our predictions and the simulations from Lanzerath. The same trends seem reasonable because our adsorber model uses the same assumptions as the model from Lanzerath. However, the same trends for our predictions and the simulations from Lanzerath imply that further improvement of the prediction cannot be achieved from more accurately determined heat transfer and diffusion coefficients. Yet, a profound statement can only be made, if the heat transfer and diffusion coefficients in our distributed parameter model would also be fitted directly to the full-scale adsorption chiller experiment. However, the high computational time (approximately 24 h for one simulation of the full-scale adsorption chiller model) does not allow to find the optimal heat transfer and diffusion coefficients at the moment by fitting to the full-scale adsorber.

The high computational time of the full-scale adsorption chiller model also limits its immediate application to optimize the adsorber geometry. For this purpose, model reductions, as already proposed by different discretizations of the adsorber bed and the tube in longitudinal direction (cf., Section 2.2), need to be further implemented. To this end, a representative adsorber part could be implemented instead of a full-scale adsorber. In the representative adsorber part, only a short tube could be modeled. In addition, models of an ideal evaporator and condenser could be implemented to further reduce computational time. The resulting model would allow optimizing the adsorber geometry for the investigated working pair/adsorbent configuration.

In summary, the presented full-scale adsorption chiller model predicts the COP, the SCP, and even the heat flow rates with remarkable accuracy. For these results, only small-scale IR-LTJ experiments are necessary. With our presented method, calibration of adsorber models with data from full-scale experiments is not required.

4. Conclusions

Adsorption chillers are still characterized by large-scale experiments today. To reduce time and material needs, we present a

method to reliably predict the performance of a working pair and an adsorber geometry regarding the heat flows in the adsorber, SCP, and COP in an adsorption chiller.

For this purpose, we combine the small-scale IR-LTJ method with a distributed parameter model of a full-scale adsorption chiller. This combination allows determining the heat flows in the adsorber, SCP, and COP of a working pair for a variety of adsorber geometries with high accuracy from only a small adsorbent mass of 1 g.

We conduct two IR-LTJ experiments with different adsorbent bed heights. Varying the bed height allows distinguishing between the effective heat transfer between the heat exchanger and the adsorbent bed $U_{\text{sor-hx,eff}}$ and the effective heat conductivity within the adsorbent bed $k_{\text{sor,eff}}$. In addition, the effective diffusion coefficient D_{eff} is determined. To this end, measured and simulated pressure and adsorbent temperature are fitted by least square.

In a case study, we investigate the working pair silica gel 123/water with a mean particle size of $d_{\text{particle}} = 0.9$ mm in a packed-bed configuration. We perform the IR-LTJ experiments for the temperature set of 10/30/80 °C, and determine the heat transfer and diffusion coefficients.

We use the heat transfer and diffusion coefficients to parameterize a full-scale adsorption chiller model. The adsorption chiller model allows determining the heat flows in the adsorber and the performance in terms of the SCP and the COP for multiple adsorber geometries. Comparison with literature and experimental data shows excellent prediction capabilities of our adsorption chiller model. The average coefficient of variation, as a measure for the transient heat flow rates in the adsorber, is with 18.5% in the same range as in the literature. However, the literature model has been calibrated to a full-scale experiment, whereas our model uses only data from the small-scale IR-LTJ experiment. The predicted SCP varies by only 1.4% on average and the COP by only 7.0% compared with the experimental SCP and COP for a variety of adsorption and desorption times and temperatures in the adsorption chiller. All deviations of SCP and COP lie within the measurement uncertainty of the experiment.

The excellent accuracy achieved for the studied system suggests that the presented method allows reliably predicting the performance of working pairs and adsorber geometries in a full-scale adsorption chiller model. The methodology has been validated for a single setup due to the data availability. It would certainly be desirable to study further adsorption chillers to analyze the application range of the present methodology.

For this purpose, only small-scale IR-LTJ experiments with 1 g of adsorbent are necessary, instead of full-scale adsorption chiller experiments with usually several kilograms of adsorbent needed. Thus, the presented method allows evaluating new working pairs and adsorbent configurations at an early stage of material development.

Supporting Information

Supporting Information is available from the Wiley Online Library or from the author.

Acknowledgements

This work was conducted within the project “TailorSorb – Tailored adsorbents for stationary adsorption thermal energy transformation” (03SF0515A). The project was funded by the German Federal Ministry of Education and Research (BMBF) within the funding priority “Materialforschung für die Energiewende.”

Conflict of Interest

The authors declare no conflict of interest.

Keywords

dynamic modeling, heat transfer and diffusion mechanisms, infrared-large-temperature-jump experiment, silica gel/water

Received: September 23, 2019

Revised: November 30, 2019

Published online:

- [1] F. Meunier, *Appl. Therm. Eng.* **2013**, 61, 830.
- [2] J. Albers, A. Kühn, S. Petersen, F. Ziegler, *Chem. Ing. Tech.* **2011**, 83, 1853.
- [3] H. Demir, M. Mobedi, S. Ülkü, *Renewable Sustainable Energy Rev.* **2008**, 12, 2381.
- [4] Y. I. Aristov, *Appl. Therm. Eng.* **2014**, 72, 166.
- [5] G. Li, S. Qian, H. Lee, Y. Hwang, R. Radermacher, *Energy* **2014**, 65, 675.
- [6] Z. Zhang, Z.-Z. Yao, S. Xiang, B. Chen, *Energy Environ. Sci.* **2014**, 7, 2868.
- [7] C. Y. Tso, C. Y. Chao, S. C. Fu, *Int. J. Heat Mass Transfer* **2012**, 55, 7596.
- [8] G. Santori, A. Sapienza, A. Freni, *Renewable Energy* **2012**, 43, 301.
- [9] F. Lanzerath, U. Bau, J. Seiler, A. Bardow, *Sci. Technol. Built Environ.* **2015**, 21, 248.
- [10] U. Bau, F. Lanzerath, M. Gräber, S. Graf, H. Schreiber, N. Thielen, A. Bardow, in *Proc. of the 10th Int. Modelica Conf., Linköping Universitet, Linköping* **2014**, pp. 875–883.
- [11] L. Gong, R. Wang, Z. Xia, C. Chen, *Energy Convers. Manage.* **2011**, 52, 2345.
- [12] Y. Hamamoto, K. A. Alam, A. Akisawa, T. Kashiwagi, *Int. J. Refrig.* **2005**, 28, 344.
- [13] U. Bau, P. Hoseinpoori, S. Graf, H. Schreiber, F. Lanzerath, C. Kirches, A. Bardow, *Appl. Therm. Eng.* **2017**, 125, 1565.
- [14] A. R. Rezk, R. K. Al-Dadah, *Appl. Energy* **2012**, 89, 142.
- [15] A. Sharaifan, M. Bahrani, *Renewable Sustainable Energy Rev.* **2015**, 48, 857.
- [16] M. Schickentanz, T. Núñez, *Int. J. Refrig.* **2009**, 32, 588.
- [17] X. Wang, Z. He, H. T. Chua, *Int. J. Refrig.* **2015**, 52, 32.
- [18] H. Chua, K. Ng, W. Wang, C. Yap, X. Wang, *Int. J. Heat Mass Transfer* **2004**, 47, 659.
- [19] W. S. Teng, K. C. Leong, A. Chakraborty, *Renewable Sustainable Energy Rev.* **2016**, 63, 315.
- [20] A. Pesaran, H. Lee, Y. Hwang, R. Radermacher, H.-H. Chun, *Energy* **2016**, 100, 310.
- [21] Y. I. Aristov, *Appl. Therm. Eng.* **2012**, 42, 18.
- [22] Y. I. Aristov, *Int. J. Refrig.* **2009**, 32, 675.
- [23] I. S. Gernik, Y. I. Aristov, *Energy* **2016**, 114, 767.
- [24] A. Sakoda, M. Suzuki, *J. Chem. Eng. Jpn.* **1984**, 17, 52.
- [25] N. Douss, F. E. Meunier, L. M. Sun, *Ind. Eng. Chem. Res.* **1988**, 27, 310.
- [26] S.-H. Cho, J.-N. Kim, *Energy* **1992**, 17, 829.
- [27] L. Z. Zhang, L. Wang, *Energy* **1999**, 24, 605.
- [28] W.-D. Wu, H. Zhang, D.-W. Sun, *Appl. Therm. Eng.* **2009**, 29, 645.
- [29] M. Mahdavihah, H. Niazmand, *Appl. Therm. Eng.* **2013**, 50, 939.
- [30] A. Sapienza, S. Santamaria, A. Frazzica, A. Freni, Y. I. Aristov, *Appl. Energy* **2014**, 113, 1244.
- [31] S. Graf, F. Lanzerath, A. Sapienza, A. Frazzica, A. Freni, A. Bardow, *Appl. Therm. Eng.* **2016**, 98, 900.
- [32] S. Graf, F. Lanzerath, A. Bardow, *Appl. Therm. Eng.* **2017**, 126, 630.
- [33] Y. I. Aristov, B. Dawoud, I. S. Glaznev, A. Elyas, *Int. J. Heat Mass Transfer* **2008**, 51, 4966.
- [34] A. Freni, G. Maggio, F. Cipit, Y. I. Aristov, *Appl. Therm. Eng.* **2012**, 44, 69.
- [35] M. M. Dubinin, *J. Colloid Interface Sci.* **1967**, 23, 487.
- [36] E. Glueckauf, *Trans. Faraday Soc.* **1955**, 51, 1540.
- [37] P. A. Fritzson, *Principles of Object-Oriented Modeling and Simulation with Modelica 2.1*, 1st ed., IEEE Press and Wiley-Interscience, Piscataway **2004**.
- [38] M. Gräber, K. Kosowski, C. Richter, W. Tegethoff, *Math. Comput. Modell. Dyn. Syst.* **2010**, 16, 195.
- [39] E. W. Lemmon, M. L. Huber, M. O. McLinden, *NIST Standard Reference Database 23: Reference Fluid Thermodynamic and Transport Properties-REFPROP, Version 9.1*, National Institute of Standards and Technology, Standard Reference Data Program, Gaithersburg **2013**.
- [40] J. D. Cox, D. D. Wagman, V. A. Medvedev, *CODATA Key Values for Thermodynamics*, Hemisphere Publishing Corp., New York **1989**.
- [41] M. W. Chase, *NIST-JANAF Thermochemical Tables*, Journal of Physical and Chemical Reference Data Monographs or Supplements, 4th ed., AIP Press, New York **1998**.
- [42] N. B. Amar, L. M. Sun, F. E. Meunier, *Appl. Therm. Eng.* **1996**, 16, 405.
- [43] S. Santamaria, A. Sapienza, A. Frazzica, A. Freni, I. S. Gernik, Y. I. Aristov, *Appl. Energy* **2014**, 134, 11.
- [44] V. Brancato, L. Gordeeva, A. Sapienza, A. Freni, A. Frazzica, *Appl. Therm. Eng.* **2016**, 105, 28.
- [45] P. J. Fleming, J. J. Wallace, *Commun. ACM* **1986**, 29, 218.
- [46] F. Lanzerath, Ph.D. Thesis, Rheinisch-Westfälisch Technische Hochschule Aachen **2013**.
- [47] VDI-Gesellschaft Verfahrenstechnik und Chemieingenieurwesen (VDI-GVC), *VDI-Wärmeatlas* (in German), 11th ed., Springer-Verlag, Berlin **2013**.
- [48] E. N. Sieder, G. E. Tate, *Ind. Eng. Chem.* **1936**, 28, 1429.
- [49] U. Bau, Ph.D. Thesis, Rheinisch-Westfälisch Technische Hochschule Aachen **2018**.
- [50] D. Schawe, Ph.D. Thesis, Universität Stuttgart **2001**.
- [51] J. Gurgel, L. A. Filho, P. Grenier, F. Meunier, *Adsorption* **2001**, 7, 211.
- [52] H. Demir, M. Mobedi, S. Ülkü, *Int. J. Refrig.* **2010**, 33, 714.
- [53] L. Schnabel, Ph.D. Thesis, Technische Universität Berlin **2009**.
- [54] Y. I. Aristov, I. S. Glaznev, I. S. Gernik, *Energy* **2012**, 46, 484.
- [55] A. Velte, G. Fuldner, E. Laurenz, L. Schnabel, *Energies* **2017**, 10, 1130.
- [56] I. S. Glaznev, Y. I. Aristov, *Int. J. Heat Mass Transfer* **2010**, 53, 1893.
- [57] E. F. Schmidt, *Chem. Ing. Tech.* **1967**, 39, 781.